Nanoscale Friction of CVD Single-Layer MoS_2 with Controlled Defect Formation

Min Gi Choi,[a] Alex Belianinov,[b] Alison Pawlicki,[b,c] Seonha Park,[a] Habeom Lee,[a] Olga S. Ovchinnikova,[b,d] and Songkil Kim[a,*]

[a]School of Mechanical Engineering, Pusan National University, Busan 46241, South Korea

[b]Center for Nanophase Materials Sciences, Oak Ridge National Laboratory, Oak Ridge, TN 37831, USA

[c]Bredesen Center for Interdisciplinary Research, University of Tennessee, Knoxville, 416 Circle Drive, Knoxville, TN 37996, USA

[d]Computational Sciences and Engineering Division, Oak Ridge National Laboratory, Oak Ridge, TN 37831, USA

*Corresponding author.
E-mail address: songkil.kim@pusan.ac.kr (S. Kim).

ABSTRACT

Two-dimensional (2D) layered nanomaterials such as graphene, molybdenum disulfide (MoS_2), or tungsten disulfide offer a promising solution in areas of solid-state lubrication, due to their excellent mechanical properties as well as low friction. However, defects can influence their friction and reduce their superior tribological properties. Thus, it is crucial to understand the effects of defects on sliding behavior in 2D nanomaterials, to foster a functional strategy for utilizing 2D nanomaterials as solid-state tribological films. In this study, frictional effects of defects, grain boundaries, and atomic-scale structural defects were explored on chemical vapor deposition (CVD) grown single layer MoS_2. Selective patterning of defects into MoS_2 was accomplished *via* controlled irradiation of helium ions with varying ion doses. The friction of MoS_2 was characterized by friction force microscopy (FFM) and was found that friction depends on the defect formation controlled by helium ion irradiation. This approach offers a correlation between surface topography, defects and friction. Understanding the relative friction of MoS_2 in the

presence of different levels of defects is foundational to studying tribological properties of a single layer MoS_2 at both nanoscales and macroscales.

KEYWORDS: molybdenum disulfide (MoS_2), nanoscale friction, controlled defect formation, helium ion beam irradiation, friction force microscopy (FFM)

1. Introduction

Roughly 30% of the world's generated energy is wasted due to various types of mechanical friction every year [1-3]. Friction is the origin of wear, tear and eventual failure of mechanical systems, making its elimination a lucrative economic proposition [4]. Lubrication strategies depend on application environment. Liquid lubrication, which provides high tribological performance, cannot be used in all mechanical systems. In harsh environments, space crafts, and micro/nano systems – where liquid lubrication cannot be utilized – solid-state lubricants can replace liquid lubricants [5]; but dry friction in solid-state lubricants is generally higher than in their liquid counterparts. Therefore, materials for high-performance solid-state lubricants, ideally demonstrating superlubricity, attract interest and research in tribology community [6, 7].

Two-dimensional (2D) nanomaterials, which are crystalline structures a few atomic layers thick, have been explored in various areas of research due to their excellent optical, electrical and mechanical properties. Among this diverse material group, graphene and molybdenum disulfide (MoS_2) have been studied extensively as solid-state lubricants due to their intrinsically excellent tribological and anti-wear properties [8-16]. Most of the studies have been focused on demonstrating the fundamental frictional characteristics of mechanically exfoliated 2D nanomaterials on SiO_2/Si substrates, using friction force microscopy (FFM). They include the mechanisms of nanoscale friction as a function of thickness (layer)-dependence and friction anisotropy [14, 17, 18]. Research shows that the friction of 2D nanomaterials

decreased with the increase in the number of layers and is attributed to various factors, such as adhesion with an underlying substrate, interface structure, and out-of-plane stiffness.[14] In addition, frictional anisotropy was discovered in mechanically exfoliated graphene and MoS_2 using FFM, where the underlying mechanism was proposed to be ripples in domains. These ripples lead to anisotropic puckering and increased contact surface area with an atomic force microscopy (AFM) tip [17].

Although there are many studies on the nanoscale friction of small (few, or tens of micrometers), defect-free, mechanically exfoliated samples; offering insight into the friction of 2D nanomaterials as well as molecular-level frictional behavior as solid-state lubricants; the research is sparse on CVD grown graphene or MoS_2. CVD grown materials enable wafer-scale synthesis, which can be directly grown or indirectly transferred onto a large area of target substrates as solid-state tribological films.[19-22] However, unlike mechanical exfoliation, CVD grown 2D nanomaterials have polycrystalline domains with grain boundaries [23, 24], as well as a variety of defects and surface contaminants, including wrinkles and atomic structural defects, which may play a role in the material's surface friction [21, 22, 25].

In this work, we explore nanoscale friction of CVD grown single layer MoS_2. A continuous single layer MoS_2 film grown on a SiO_2/Si substrate has multiple grains and grain boundaries where friction was found to be significantly different; specifically, friction at grain boundaries can be similar to the base substrate. To investigate the effect of defects on the friction of MoS_2, we intentionally introduced different levels of defects by precisely controlled helium ion irradiation in a helium ion microscope (HIM) as described by the schematic in Figure 1. A focused helium ion beam has a minimum diameter of ~0.5 nm [26], allowing for high resolution nanomaterial imaging and milling [27-30]. Helium ion dose can also be controlled resulting in precise irradiation outcomes in localized areas of crystalline structures, with helium ion implantation, atomic lattice distortion, vacancy formation, amorphization, and sputtering/milling [31-37]. We used a 25 keV beam and doses ranging from 10^{13} to 5×10^{16} ions/cm^2, spanning a level of material damage where at the lower end, no observable change in Raman spectroscopic measurements occurred,

to complete sputtering of the MoS_2 film. The relative friction of the irradiated MoS_2 film was qualitatively investigated via FFM, which demonstrated a transitional change with the different levels of defect formation.

2. Methods

2.1. Helium ion beam imaging and irradiation

The helium ion microscope (HIM, Zeiss Orion NanoFab) was utilized for both high-resolution imaging and the irradiation experiments of the CVD single layer MoS_2 sample purchased from a vendor (6CarbonTehcnology, www.6carbon.com), using a helium ion beam with an acceleration voltage of 25 kV. The helium ion microscope chamber was pumped to a high vacuum at a pressure of ~3×10^{-7} Torr for both imaging and the irradiation experiments. The two irradiation experiments were conducted by exposing ions on a 2×3 array of square patterns with the beam current of ~5 pA and irradiation spot-to-spot distance of 10 nm×10 nm for a various dwell time, which makes different ion irradiation doses ranging from 10^{13} to 5×10^{16} ions/cm^2.

2.2. Atomic force microscopy imaging

All the surface topography and lateral deflection imaging of MoS_2 in this work were conducted using a NanoIR2-s AFM, commercially available from Anasys Instruments, Santa Barbara, CA, with the same highly doped silicon tip (tip radius below 10 nm, spring constant of 0.2 N/m and resonance frequency of 13 kHz) in a contact mode. The surface topography and lateral deflection were imaged with a resolution of 256×256 or 512×512. The AFM set point (relevant to a normal load applied to the sample by an AFM tip) and scan speed were varied for 0.55~0.91 V and 0.3~0.5 Hz, respectively, but the AFM settings were maintained constant within an AFM image. The lateral deflection images obtained from the AFM scans in the trace and retrace directions were subtracted and divided by two to extract friction images and surface

line profiles of friction signals. The variation of the AFM scan settings including laser alignment, scan speed and applied load (set point) can result in different lateral deflection signal amplitudes even on the same material domain, but the lateral deflection signals within the image is sufficient to provide the qualitative analysis for the difference in friction along different material domains of interests. The analysis for friction between two different images were conducted by considering relative friction to the same referenced material domain, which is also reasonable to compare the friction. Imaging processing of all the AFM images was implemented using Gwyddion version 2.53.

3. Results and discussion

Figure 2 shows the HIM images of CVD single-layer MoS_2 grown on the SiO_2/Si substrate. Most of the area is a continuous film as shown in Figure 2(a). The bright areas in Figure 2(b) are the MoS_2 film and the dark areas are the substrate. Additionally, optical microscopy images of the MoS2 film are provided in the supplementary material Figure S1 to verify that the film is mostly continuous and monolayer. The surface of the MoS_2 film has some contaminants, possibly deposited during the synthesis which may attribute to the increase in surface friction of the MoS_2, as shown in the supplementary material (Figure S2).

Figure 3 shows the surface topography and friction images of MoS_2, using FFM. FFM is a subset of a contact-mode AFM where a cantilever tip is rastered across a sample surface, producing a vertical and lateral deflection images simultaneously. Vertical deflection images reflect the sample topography whereas lateral deflection images contain information on the surface friction, which enables the identification of different material domains and grain boundaries. The lateral deflection images obtained from the AFM scans in the trace and retrace directions were subtracted and divided by two to extract friction images. It is worth noting that the variation of the AFM scan settings can result in different lateral deflection signal amplitudes even on the same material domain, but the lateral deflection signals over the

same scanned image, which means the same AFM scan settings, is sufficient to provide qualitative analysis of friction along the different material domains of interests. Figures 3(a) and 3(b) show the surface topography and the corresponding friction images of a continuous MoS_2 region, while the imaging results of a MoS_2/SiO_2 interface are provided in Figures 3(c) and 3(d). Grain boundaries of MoS_2 are where two adjacent crystalline domains (grains) meet together during a growth process, which has a different atomic structure but no measurable topographic change from the crystalline domains. Thus, the grain boundaries can be considered as atomic defects relative to the crystalline domains. Due to the defected nature of the grain boundaries, they have different interaction with an AFM tip during scanning, and thus, the friction imaging enables the identification of grain boundaries. Figure 3(b) shows the friction image of MoS_2, which clearly shows the distribution of grain boundaries, while no topographic difference of grain boundaries is observed in the surface topography image of Figure 3(a). Figures 3(c) and 3(d) show the surface topography and friction images of the interface between MoS_2 and the SiO_2/Si substrate, respectively. The step height at the interface was measured as 1.0±0.4 nm, which confirms a single layer of MoS_2. (see the supplementary material, Figure S3) The friction image in Figure 3(d) demonstrates the different surface friction arising from the different material domains. The difference in friction between MoS_2 and the substrate can be unambiguously identified, demonstrating a much lower friction on MoS_2 than the SiO_2. Figure 3(e) compares the friction signals of the grain boundary and SiO_2 relative to the signals on the crystalline domain of MoS_2, along the white dashed line in Figures 3(b) and 3(d). The relative friction on the grain boundary and SiO_2 are approximately four times higher than that of the crystalline domain, which indicates that the grain boundary on MoS_2 can result in a similar level of friction to the SiO_2 and implies that the friction of a MoS_2 film can be greatly influenced by the density of grain boundaries.

MoS_2 can have various types of defects including grain boundaries, S and Mo vacancies, lattice disorder, and so on, which can be generated during synthesis or by mechanical forces in operation as a

solid-state tribological film. Since the formation of defects can influence the tribological performance of MoS_2, it is important to understand the effect of nanoscale defects on its friction. To study the effect of defect formation on the friction of MoS_2, we intentionally generated defects by helium ion irradiation. Helium ion irradiation affects MoS_2 differently depending on a beam energy and an irradiation dose, resulting in the formation of atomic defects such as S or Mo vacancies to the continuous increase of the structural disorder finally to be sputtered at a large extent [36-40]. For example, the structural evolution of MoS_2 under helium ion irradiation at the energy of 25 keV or 30 keV occurs with respect to the ion dose range of 10^{13}~10^{18} ions/cm^2 [36]. Leveraging the density of atomic defects by controlling the helium ion irradiation dose, which can give rise to the stronger interaction (higher adhesive force) with a counter-part material (an approaching AFM tip in this work), can lead to the increased friction of MoS_2 [25].

The helium ion irradiation was conducted using a Zeiss Orion NanoFab HIM. Six 3 μm × 3 μm squares were exposed to helium ions at an energy of 25 kV and ~5 pA beam current with ion irradiation doses ranging from 10^{13} to 5×10^{16} ions/cm^2. Two sets of irradiation experiments were performed and the results are shown in Figure 4 and Figure S4. Figure 4 shows surface topography and friction images of the MoS_2 film after the patterned helium ion irradiation with a dose from 5×10^{13} to 5×10^{16} ions/cm^2. Figure S3 shows the results with a dose ranging from 10^{13} to 10^{16} ions/cm^2. As shown in Figure 4(a), for the first two square patterns irradiated with ion doses of 5×10^{13} and 10^{14} ions/cm^2, there was no significant surface topographic change. Increasing the irradiation ion dose of 5×10^{14} and 10^{15} ions/cm^2 resulted in the change of surface topography, leading to the increase of surface roughness by incomplete milling of MoS_2. Further increasing the ion dose above 10^{16} ions/cm^2 resulted in the complete milling of the MoS_2 and exposing the substrate. The milled depths were measured as ~4.3 nm and ~5.1 nm for the ion dose of 10^{16} and 5×10^{16} ions/cm^2, respectively, which confirms the complete milling of the MoS_2 film as well as the partial sputtering of the substrate underneath.

Figure 4(b) shows the friction image of the MoS_2 film corresponding to the surface topography image in Figure 4(a). While no significant change was observed in the surface topography, the distinct frictional patterns can be identified at the low ion dose conditions. It highlights that helium ion irradiation can engineer the surface friction of MoS_2 without any observable topographic change by properly controlling the irradiation conditions. At the ion dose of 5×10^{14} ions/cm^2, the surface topography of the sputtered MoS_2 led to the significant increase in the friction as compared to the unexposed or lower ion dose irradiated MoS_2. At an increase ion dose above 10^{16} ions/cm^2, the friction comes from the helium ion irradiated SiO_2 substrate. Figure 5 shows the high-resolution images and cross-sectional profiles for the square patterns irradiated at a dose of 10^{14} and 5×10^{14} ions/cm^2, respectively. As seen in Figures 5(a)-5(c), it is clear that no topographic change is observed at a dose of 10^{14} ions/cm^2 while the relative frictional signal is measured as much as ~6 mV higher than the surrounding unexposed region of MoS_2. At an irradiation dose of 5×10^{14} ions/cm^2, more prominent increase of the relative friction signal on the square pattern was measured as ~15 mV higher than the unexposed MoS_2. The similar trend was observed in another set (ion dose range of 10^{13} ~10^{16} ions/cm^2) of the irradiation experiments whose results are provided in the supplementary material (Figure S4). That is, the relative friction increases with increasing ion dose which results in atomic defect formation to the partial sputtering of MoS_2 and the relative friction is reduced at an ion dose of 10^{16} ions/cm^2 by the complete mill of MoS_2. It is worth noting that during the helium ion irradiation, the interaction of incident helium ion beam-induced secondary electrons with hydrocarbon molecular adsorbents over the substrate can deposit a thin carbon film, which can influence surface properties of MoS_2. However, the surface concentration of hydrocarbon molecular adsorbents is low since the irradiation experiment was conducted in a high vacuum at a pressure of ~3×10^{-7} Torr and the sample was stored in the HIM chamber at least for five hours before starting the irradiation experiments. At the low level of hydrocarbon molecules, the deposition occurs under the surface diffusion limited regime resulting in carbon deposition surrounding the irradiated region by a long range of the

secondary electron spatial distribution and then an apparent carbon film formed with a sufficient ion dose. Since our experimental observation with a dose range of 10^{13}~5×10^{16} ions/cm^2 indicates no topographic evidence for carbon deposition, rather the milling out of the substrate, we can conclude that no carbon is deposited and the effect of carbon deposition on the relative friction of helium ion-irradiated MoS_2 is negligible.

To summarize the effects of defect formation on the frictions of MoS_2, the relative friction signal of each square pattern, normalized to the helium ion irradiated SiO_2 substrate (square pattern exposed at the highest ion dose), are plotted as a function of the irradiation dose as shown in Figure 6(a). Figure 6(b) shows the magnified plot for the ion dose range of 0~10^{15} ions/cm^2 to present the effect of helium ion irradiation more clearly. The irradiation data set 1 and set 2 in Figure 6 represents the results from the irradiation experiments shown in Figure 4 and Figure S4, respectively. The relative friction signal was normalized since the measured signal can vary by AFM imaging conditions such as a set point (normal force on the sample by an AFM tip) and a scan speed. Three distinct ranges of ion irradiation doses are identified as seen in Figure 6. At an ion dose range of 0~10^{14} ions/cm^2, the linear increase of the friction without the observable surface topographic change, which results from the increased density of atomic defects. At a dose below 10^{15} ions/cm^2 but higher than 10^{14} ions/cm^2, the friction is influenced by the combinatorial effect of the significantly damaged MoS_2 and the underneath substrate with a surface roughness whose root-mean-square (rms) roughness is around ~1.7 nm. Further increasing irradiation dose higher than 10^{15} ions/cm^2 milled out MoS_2 completely and also partially sputtered the substrate resulting in the smoother surface whose rms roughness is reduced as ~1.1 nm and ~0.8 nm after irradiation at a dose of 10^{16} and 5×10^{16} ions/cm^2, respectively and finally reducing the relative surface friction.

4. Conclusions

In conclusion, we present a novel approach to screen the effect of defects on the friction of a single layer MoS_2. The approach is to use finely controlled helium ion irradiation to generate different levels of defects on MoS_2 and to investigate the resulting friction with FFM. Remarkably, a low density of atomic defects on MoS_2, with a helium ion dose of 10^{13} ions/cm^2, can result in the significant increase of friction, even though MoS_2 maintains its 2D nature of structural integrity at nanoscale. With an increased helium ion dose, beyond that of inducing a low density of atomic defects, the MoS_2 film is sputtered which increases the surface roughness and friction with the combinatorial effect of surface topography as well as stronger interaction between damaged MoS_2 and the AFM tip [25]. This work demonstrates a distinct nanoscale mechanism of surface friction change of MoS_2 under external energy input inducing defect formation and also suggests the significance of a MoS_2 film synthesis achieving high structural and compositional integrity with defect-free and large-area crystalline domains (that is, low density of grain boundaries) as solid-state tribological applications, while a MoS_2 film by itself is known to have very low friction and a superior tribological performance. In addition, we also highlight the capability for selective nanoscale patterning of friction on MoS_2 with the controlled helium ion irradiation, which can provide intriguing opportunities to any application such as micro/nano mechanical systems or energy harvesting systems, possibly requiring the control of frictions.

Declaration of Competing Interest

The authors declare that they have no known competing financial interests or personal relationships that could have appeared to influence the work reported in this paper.

ACKNOWLEDGEMENTS

This research was conducted at the Center for Nanophase Materials Sciences, which is a Department of Energy (DOE) Office of Science User Facility. Research was supported primarily by the National

Research Foundation of Korea (NRF) grant funded by the Korea government (MSIT) (No. 2019R1C1C1010556) and by the National Research Foundation of Korea (NRF) grant funded by the Korea government (MSIT) (No. 2019R1A5A8083201), and partially by 2020 BK21 FOUR Program of Pusan National University.

Appendix A. Supplementary material

The supplementary material is available for this paper showing optical microscopy images and additional HIM images of the CVD single layer MoS_2 sample and the AFM imaging results demonstrating the monolayer thickness of the MoS_2 sample as well as the results of the irradiation experiment 2.

REFERENCES

1. P. Huang, Q. Yang, Theory and contents of frictional mechanics, Friction **2**(1) (2014) 27-39. https://doi.org/10.1007/s40544-013-0034-y
2. K. Holmberg, P. Andersson, A. Erdemir, Global energy consumption due to friction in passenger cars, Tribol. Int. 47 (2012) 221-234. https://doi.org/10.1016/j.triboint.2011.11.022
3. K. Holmberg, P. Andersson, N. O. Nylund, K. Mäkelä, A. Erdemir, Global energy consumption due to friction in trucks and buses, Tribol. Int. 78 (2014) 94-114. https://doi.org/10.1016/j.triboint.2014.05.004
4. S. Zhang, T. Ma, A. Erdemir, Q. Li, Tribology of two-dimensional materials: from mechanisms to modulating strategies, Mater. Today 26 (2019) 67-86. https://doi.org/10.1016/j.mattod.2018.12.002
5. L. Liu, M. Zhou, L. Jin, L. Li, Y. Mo, G. Su, X. Li, H. Zhu, Y. Tian, Recent advances in friction and lubrication of graphene and other 2D materials: mechanisms and applications, Friction 7(3) (2019) 199-216. https://doi.org/10.1007/s40544-019-0268-4

6. M. Hirano, K. Shinjo, Atomistic locking and friction, Phys. Rev. B 41(17) (1990) 11837-11851. https://doi.org/10.1103/PhysRevB.41.11837

7. K. Shinjo, M. Hirano, Dynamics of friction: superlubric state, Surf. Sci. 283 (1993) 473-478. https://doi.org/10.1016/0039-6028(93)91022-H

8. K. S. Kim, H. J. Lee, C. Lee, S. K. Lee, H. Jang, J. H. Ahn, J. H. Kim, H. J. Lee, Chemical vapor deposition-grown graphene: the thinnest solid lubricant, Acs Nano 5(6) (2011) 5107-5114. https://doi.org/10.1021/nn2011865

9. F. Wahlisch, J. Hoth, C. Held, T. Seyller, R. Bennewitz, Friction and atomic-layer-scale wear of graphitic lubricants on SiC(0001) in dry sliding, Wear 300 (2013) 78-81. https://doi.org/10.1016/j.wear.2013.01.108

10. A. L. Kitt, Z. Qi, S. Remi, H. S. Park, A. K. Swan, B. B. Goldberg, How graphene slides: measurement and theory of strain-dependent frictional forces between graphene and SiO_2. Nano Lett. 13(6) (2013) 2605-2610. https://doi.org/10.1021/nl4007112

11. S. Bertolazzi, J. Brivio, A. Kis, Stretching and breaking of ultrathin MoS_2. ACS Nano **5**(12) (2011) 9703-9709. https://doi.org/10.1021/nn203879f

12. A. Castellanos-Gomez, M. Poot, G. A. Steele, H. S. J. van der Zant, N. Agrait, G. Rubio-Bollinger, Elastic properties of freely suspended MoS_2 nanosheets. Adv. Mater. 24(6) (2012) 772-775. https://doi.org/10.1002/adma.201103965

13. J. M. Martin, Superlubricity of molybdenum disulfide, Phys. Rev. B 48(14) (1993) 10583-10586. https://doi.org/10.1016/B978-044452772-1/50044-5

14. C. Lee, Q. Li, W. Kalb, X. Z. Liu, H. Berger, R. W. Carpick, J. Hone, Frictional characteristics of atomically thin sheets, Science 328 (2010) 76-80. https://doi.org/10.1126/science.1184167

15. H. S. Sen, H. Sahin, F. M. Peeters, E. Durgun, Monolayers of MoS_2 as an oxidation protective nanocoating material, J. Appl. Phys. 116(8) (2014) 083508. https://doi.org/10.1063/1.4893790

16. A. A. Pawlicki, D. G. Bansal, N. Borodinov, A. Belianinov, K. Cogen, D. Clarke, B. G. Sumpter, O. S. Ovchinnikova, In situ multimodal imaging for nanoscale visualization of tribofilm formation, J. Appl. Phys. 127(15) (2020) 154303. https://doi.org/10.1063/1.5140480

17. J. S. Choi, J. S. Kim, I. S. Byun, D. H. Lee, M. J. Lee, B. H. Park, C. Lee, D. Yoon, H. Cheong, K. H. Lee, Y. W. Son, J. Y. Park, M. Salmeron, Friction anisotropy-driven domain imaging on exfoliated monolayer graphene, Science 333 (2011) 607-610. https://doi.org/10.1126/science.1207110

18. Y. Dong, Effects of substrate roughness and electron-phonon coupling on thickness-dependent friction of graphene, J. Phys. D: Appl. Phys. 47(5) (2014) 055305. https://doi.org/10.1088/0022-3727/47/5/055305

19. R. Munoz, C. Gomez-Aleixandre, Review of CVD synthesis of graphene, Chem. Vap. Dep. 19 (2013) 297-322. https://doi.org/10.1002/cvde.201300051

20. Y. Zhang, L. Y. Zhang, C. W. Zhou, Review of chemical vapor deposition of graphene and related applications, Acc. Chem. Res. 46(10) (2013) 2329-2339. https://doi.org/10.1021/ar300203n

21. Y. Zhan, Z. Liu, S. Najmaei, P. M. Ajayan, J. Lou, Large-area vapor-phase growth and characterization of MoS_2 atomic layers on a SiO_2 substrate, Small 8(7) (2012) 966-971. https://doi.org/10.1002/smll.201102654

22. Y. H. Lee, X. Q. Zhang, W. Zhang, M. T. Chang, C. T. Lin, K. D. Chang, Y. C. Yu, J. T. W. Wang, C. S. Chang, L. J. Li, T. W. Lin, Synthesis of large-area MoS_2 atomic layers with chemical vapor deposition, Adv. Mater. 24(17) (2012) 2320-2325. https://doi.org/10.1002/adma.201104798

23. A. M. van der Zande, P. Y. Huang, D. A. Chenet, T. C. Berkelbach, Y. M. You, G. H. Lee, T. F. Heinz, D. R. Reichman, D. A. Muller, J. C. Hone, Grains and grain boundaries in highly crystalline monolayer molybdenum disulphide, Nat. Mater. 12(6) (2013) 554-561. https://doi.org/10.1038/nmat3633

24. S. Najmaei, Z. Liu, W. Zhou, X. Zou, G. Shi, S. Lei, B. I. Yakobson, J. C. Idrobo, P. M. Ajayan, J. Lou, Vapour phase growth and grain boundary structure of molybdenum disulphide atomic layers, Nat. Mater. 12(8) (2013) 754-759. https://doi.org/10.1038/nmat3673

25. D. L. C. Ky, B. C. T. Khac, C. T. Le, Y. S. Kim, K. H. Chung, Friction characteristics of mechanically exfoliated and CVD-grown single-layer MoS_2, Friction 6(4) (2018) 395-406. https://doi.org/10.1007/s40544-017-0172-8

26. M. M. Marshall, J. J. Yang, A. R. Hall, Direct and transmission milling of suspended silicon nitride membranes with a focused helium ion beam, Scanning 34(2) (2012) 101-106. https://doi.org/10.1002/sca.21003

27. D. Cohen-Tanugi, N. Yao, Superior imaging resolution in scanning helium-ion microscopy: a look at beam-sample interactions, J. Appl. Phys. 104(6) (2008) 063504. https://doi.org/10.1063/1.2976299

28. A. Belianinov, M. J. Burch, S. Kim, S. Tan, G. Hlawacek, O. S. Ovchinnikova, Noble gas ion beams in materials science for future applications and devices, MRS Bull. 42(9) (2017) 660-666. doi:10.1557/mrs.2017.185

29. S. Kim, O. Dyck, A. V. Ievlev, I. V. Vlassiouk, S. V. Kalinin, A. Belianinov, S. Jesse, O. S. Ovchinnikova, Graphene milling dynamics during helium ion beam irradiation, Carbon 138 (2018) 277-282. https://doi.org/10.1016/j.carbon.2018.06.017

30. S. Kim, A. Trofimov, F. Khanom, L. Stern, W. Lamberti, R. Colby, D. Abmayr, A. Belianinov, O. S. Ovchinnikova, High resolution multimodal chemical imaging platform for organics and inorganics, Anal. Chem., 91(19) (2019) 12142-12148. https://doi.org/10.1021/acs.analchem.9b03377

31. J. Jadwiszczak, P. Maguire, C. P. Cullen, G. S. Duesberg, H. Zhang, Effect of localized helium ion irradiation on the performance of synthetic monolayer MoS_2 field-effect transistors, Beilstein J. Nanotechnol. 11 (2020) 1329-1335. https://doi.org/10.3762/bjnano.11.117

32. M. G. Stanford, P. R, Pudasaini, A, Belianinov, N. Cross, J. H. Noh, M. R. Koehler, D. G. Mandrus, G. Duscher, A. J. Rondinone, I. N. Ivanov, T. Z. Ward, P. D. Rack, Focused helium-ion beam irradiation effects on electrical transport properties of few-layer WSe_2: enabling nanoscale direct write homo-junctions. Sci. Rep. 6 (2016) 27276. https://doi.org/10.1038/srep27276

33. V. Iberi, A. V. Ievlev, I. Vlassiouk, S. Jesse, S. V. Kalinin, D. C. Joy, A. J. Rondinone, A. Belianinov, O. S. Ovchinnikova, Graphene engineering by neon ion beams, Nanotechnol. 27(12) (2016) 125302. https://doi.org/10.1088/0957-4484/27/12/125302

34. V. Iberi, L. Liang, A. V. Ievlev, M. G. Stanford, M.-W. Lin, X. Li, M. Mahjouri-Samani, S. Jesse, B. G. Sumpter, S. V. Kalinin, D. C. Joy, K. Xiao, A. Belianinov, O. S. Ovchinnikova, Nanoforging single layer $MoSe_2$ through defect engineering with focused helium ion beams. Sci. Rep. 6 (2016) 30481. https://doi.org/10.1038/srep30481

35. D. Seol, S. Kim, W. S. Jang, *et. al*, Selective patterning of out-of-plane piezoelectricity in $MoTe_2$ via focused ion beam, Nano Energy 79 (2021) 105451. https://doi.org/10.1016/j.nanoen.2020.105451

36. D. S. Fox, Y. Zhou, P. Maguire, A. O'Neill, C. Ó'Coileáin, R. Gatensby, A. M. Glushenkov, T. Tao, G. S. Duesberg, I. V. Shvets, M. Abid, M. Abid, H.-C. Wu, Y. Chen, J. N. Coleman, J. F. Donegan, H. Zhang, Nanopatterning and electrical tuning of MoS_2 layers with a subnanometer helium ion beam, Nano Lett. 15(8) (2015) 5307-5313. https://doi.org/10.1021/acs.nanolett.5b01673

37. M. Ghorbani-Asl, S. Kretschmer, D. E. Spearot, A. V. Krasheninnikov, Two-dimensional MoS_2 under ion irradiation: from controlled defect production to electronic structure engineering, 2D Mater. 4(2) (2017) 025078. https://doi.org/10.1088/2053-1583/aa6b17

38. S. Kretschmer, M. Maslov, S. Ghaderzadeh, M. Ghorbani-Asl, G. Hlawacek, A. V. Krasheninnikov, Supported two-dimensional materials under ion irradiation: the substrate governs defect production. ACS Appl.Mater. Interfaces 10(36) (2018) 30827-30836. https://doi.org/10.1021/acsami.8b08471

39. E. Mitterreiter, B. Schuler, K. A. Cochrane, U. Wurstbauer, A. Weber-Bargioni, C. Kastl, A. W. Holleitner, Atomistic positioning of defects in helium ion treated single-layer MoS_2, Nano Lett. 20(6) (2020) 4437-4444. https://doi.org/10.1021/acs.nanolett.0c01222

40. J. P. Thiruraman, P. M. Das, M. Drndic, Irradiation of transition metal dichalcogenides using a focused ion beam: controlled single-atom defect creation, Adv. Funct. Mater. 29(52) (2019) 1904668 https://doi.org/10.1002/adfm.201904668

Figures:

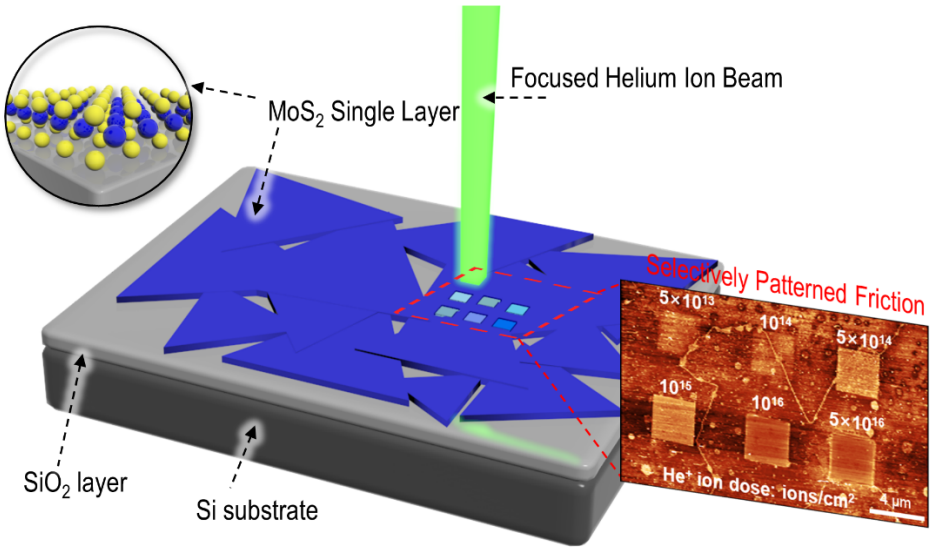

Figure 1. Schematic description of the experiment approach enabling the selectively patterned surface friction on a single layer MoS2 using precisely controlled helium ion beam irradiation.

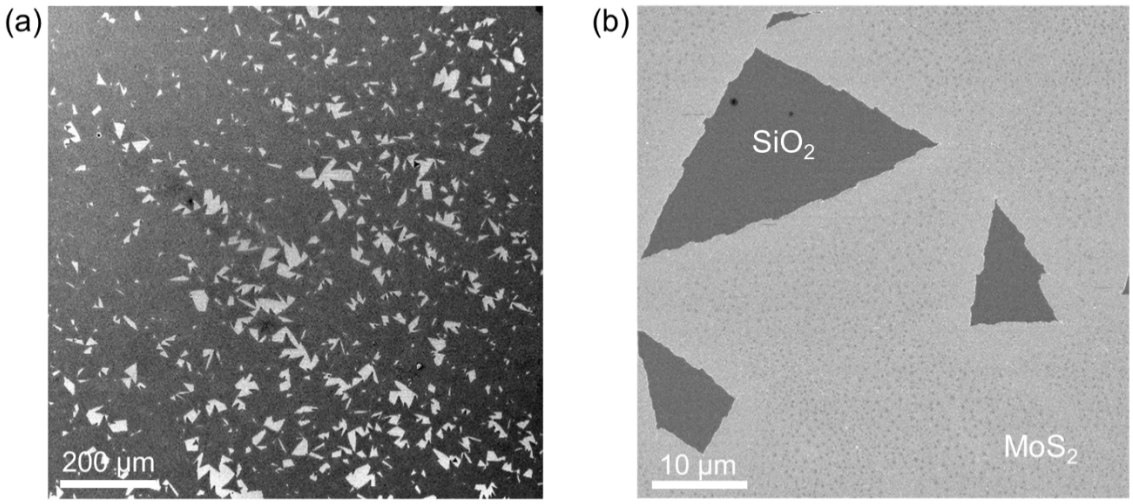

Figure 2. Helium ion microscopy secondary electron (iSE) images of a single layer MoS_2 film grown on the SiO_2/Si substrate: (a) a large-area continuous film with some discontinuities exposing the underneath substrate and (b) a high-resolution image of the MoS_2 film.

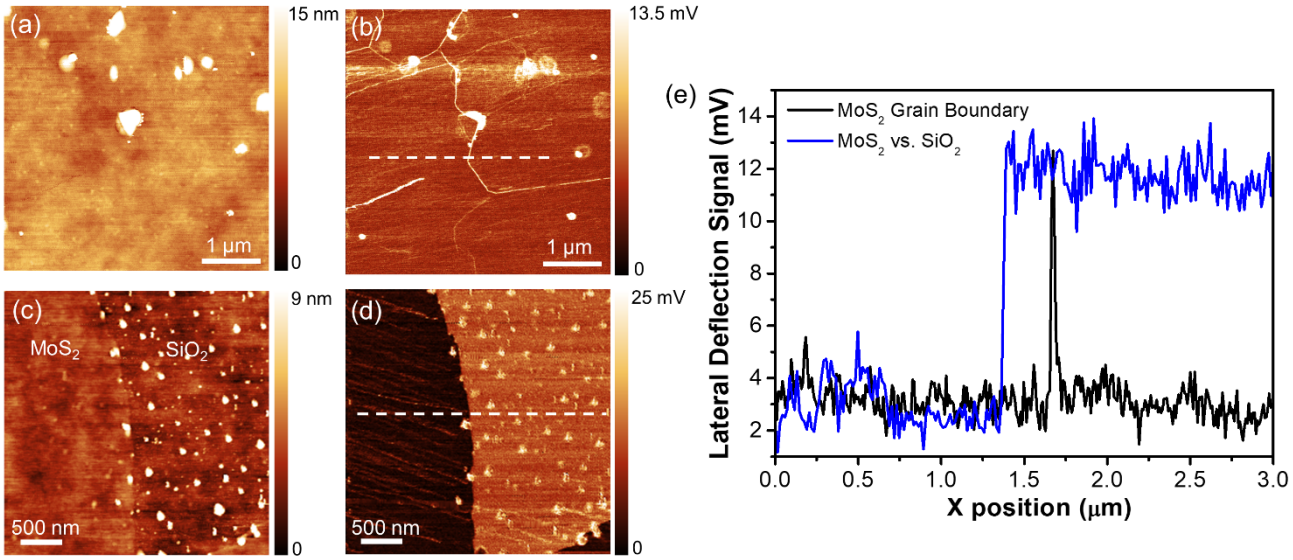

Figure 3. (a) Surface topography and (b) friction images of MoS_2 with grain boundaries, and (c) surface topography and (d) friction images of the MoS_2/SiO_2 interface. (e) Surface line profiles (white dashed lines) to compare the relative friction of MoS_2 grain boundaries *vs.* SiO_2 relative to the crystalline domain of MoS_2.

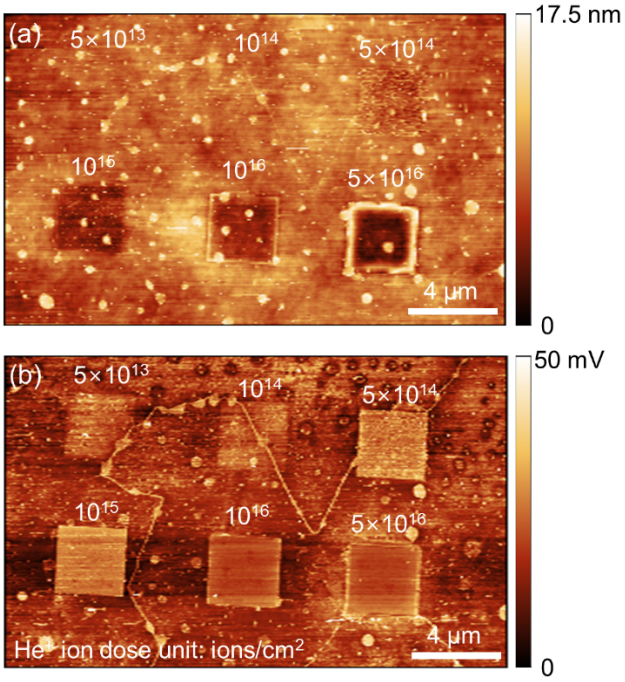

Figure 4. (a) Surface topography and (b) friction images of MoS2 patterned by controlled helium ion irradiation to demonstrate the effect of irradiation-induced defect formation on the friction of MoS_2.

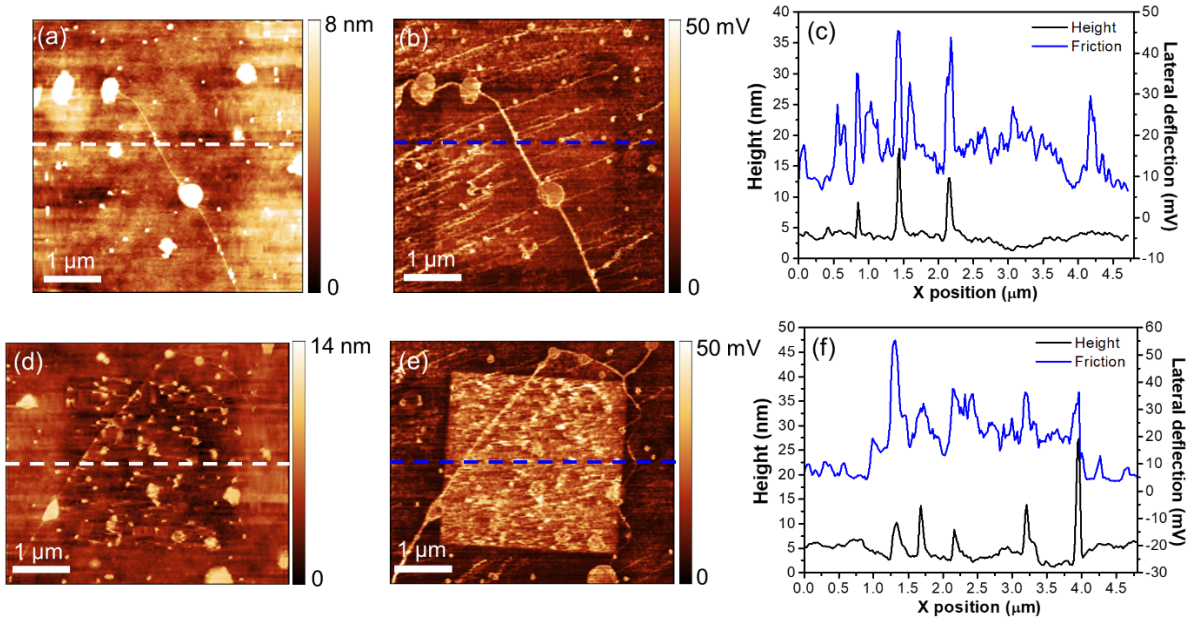

Figure 5. High-resolution surface topography and friction images of MoS_2 after helium ion irradiation: (a) surface topography and (b) friction images after ion irradiation at a dose of 10^{14} ions/cm^2 and (c) the corresponding surface line profiles, and (d) surface topography and (b) friction images after ion irradiation at a dose of 5×10^{14} ions/cm^2 and (f) the corresponding surface line profiles.

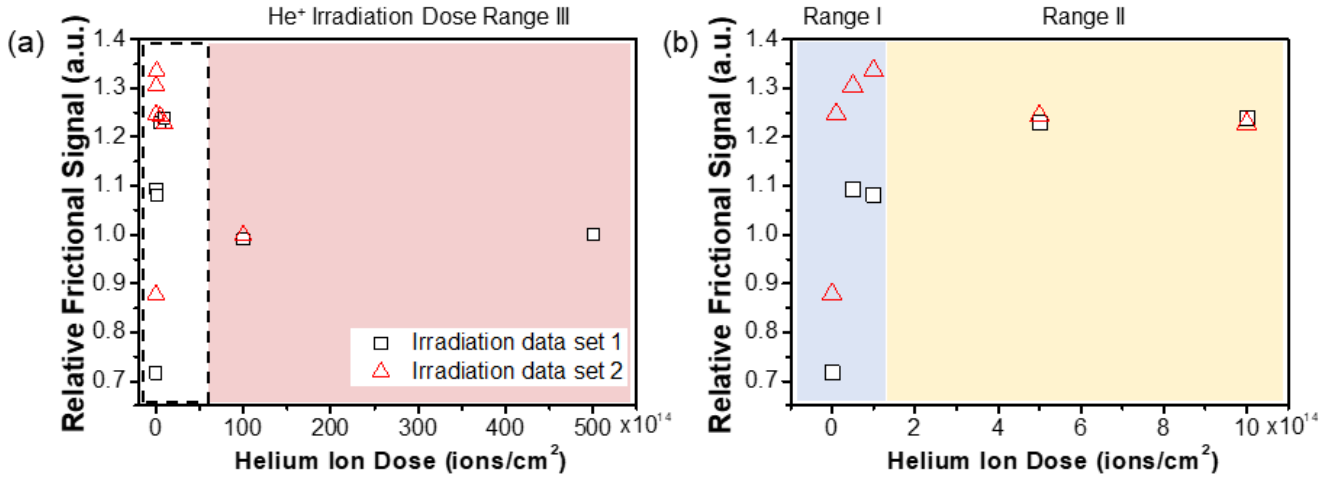

Figure 6. (a) Relative friction of MoS_2 normalized to that of the helium irradiated SiO_2/Si substrate to demonstrate the effect of helium ion irradiation dose (that is, different levels of defect formation) on the friction of MoS_2, summarized from the results done in the two irradiation experiments and (b) the magnified plot for the black dashed box in (a).

Supplementary Material for "Nanoscale Friction of CVD Single-Layer MoS_2 with Controlled Defect Formation"

Min Gi Choi,[a] Alex Belianinov,[b] Alison Pawlicki,[b,c] Seonha Park,[a] Habeom Lee,[a] Olga S. Ovchinnikova,[b,d] and Songkil Kim[a,*]

[a]School of Mechanical Engineering, Pusan National University, Busan 46241, South Korea

[b]Center for Nanophase Materials Sciences, Oak Ridge National Laboratory, Oak Ridge, TN 37831, USA

[c]Bredesen Center for Interdisciplinary Research, University of Tennessee, Knoxville, 416 Circle Drive, Knoxville, TN 37996, USA

[d]Computational Sciences and Engineering Division, Oak Ridge National Laboratory, Oak Ridge, TN 37831, USA

Figure S1 shows optical microscopy images of the MoS_2 film over the multiple areas of the sample. Figure S1(a) verifies that the film is mostly continuous and some areas near the edge of the sample substrate have a discontinuous MoS_2 film showing triangular shapes of MoS_2 flakes. Figures S1(b) and S1(c) are the magnified images, showing that the image color contrast of the MoS_2 film is uniform. In addition, the dots in red dashed circles in Figure S1(c) represent the nucleation sites which are the evidence that bi-layer MoS2 did not start to growth yet. Along with the AFM measurement of MoS_2 film thickness shown in Figure S3, it can be concluded that the film is monolayer and no bi- or tri-layer is present in our sample. Based on the optical microscopy images, we can conclude that the shape and size of grain boundaries can be arbitrarily distributed over the continuous film.

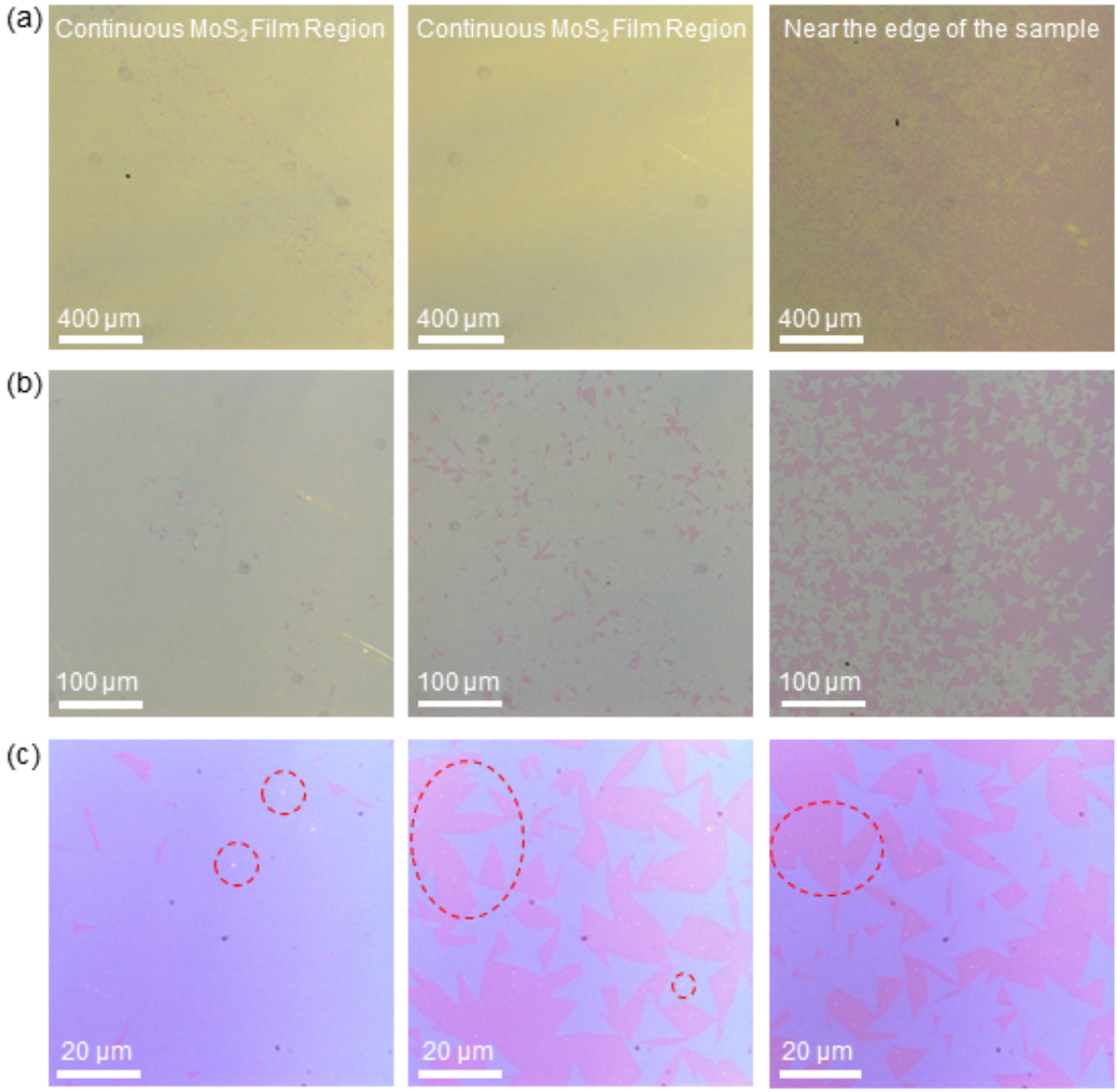

Figure S1. Optical microscopy images of the MoS_2 film with different magnifications, showing the film is mostly continuous and monolayer: (a) 50×, (b) 200× and (c) 1000×.

Figure S2 shows the HIM images of the MoS_2 film. Surface contamination over the film might be deposited during the CVD synthesis process, which can result in locally high friction over the MoS_2 film

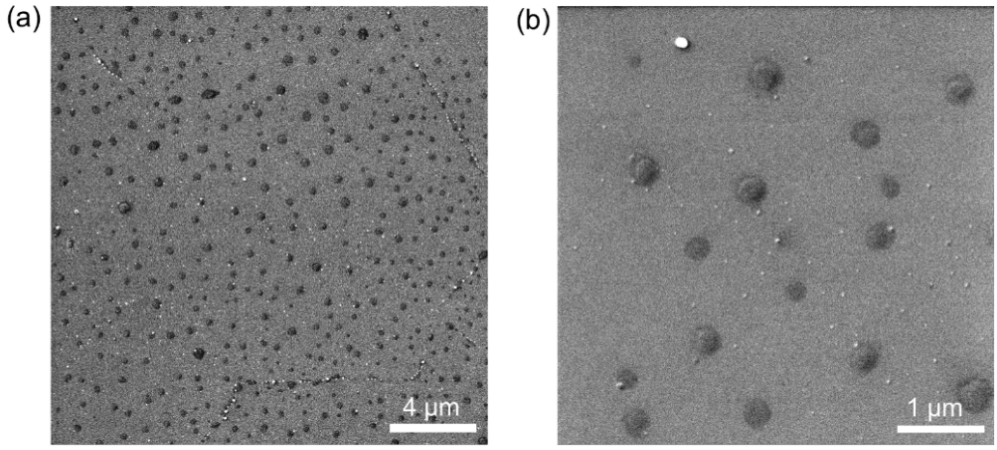

Figure S2. (a) HIM surface topography image of the MoS_2 film with (b) the zoomed-in image, showing the droplet-like surface contamination.

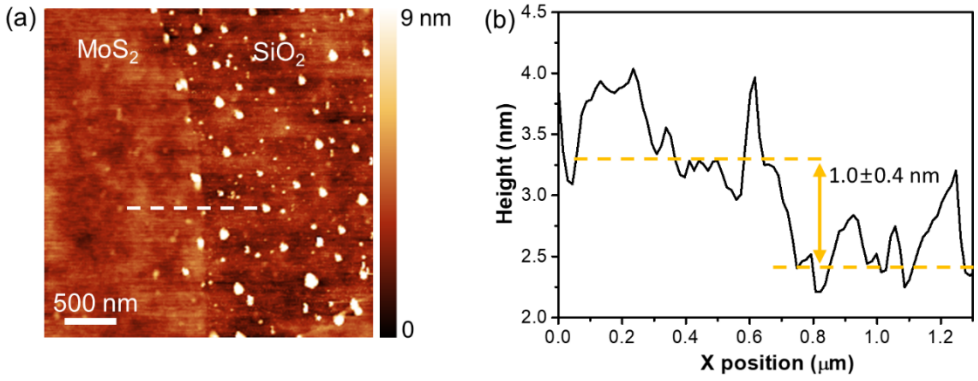

Figure S3. (a) Surface topography image of MoS_2/SiO_2 interface (b) cross-sectional profile of white dashed line. This profile shows 1.0±0.4 nm step height which indicates a single layer of MoS_2.

Figure S3 (a) shows the AFM surface topography of the interface between MoS_2 and the SiO_2/Si substrate, and the cross-sectional profile along the white dashed line in Figure S3(a) is shown in Figure S3(b). Figure S3(b) shows the step height of 1.0±0.4 nm between MoS_2 and SiO_2/Si substrate, confirming a single layer of MoS_2.

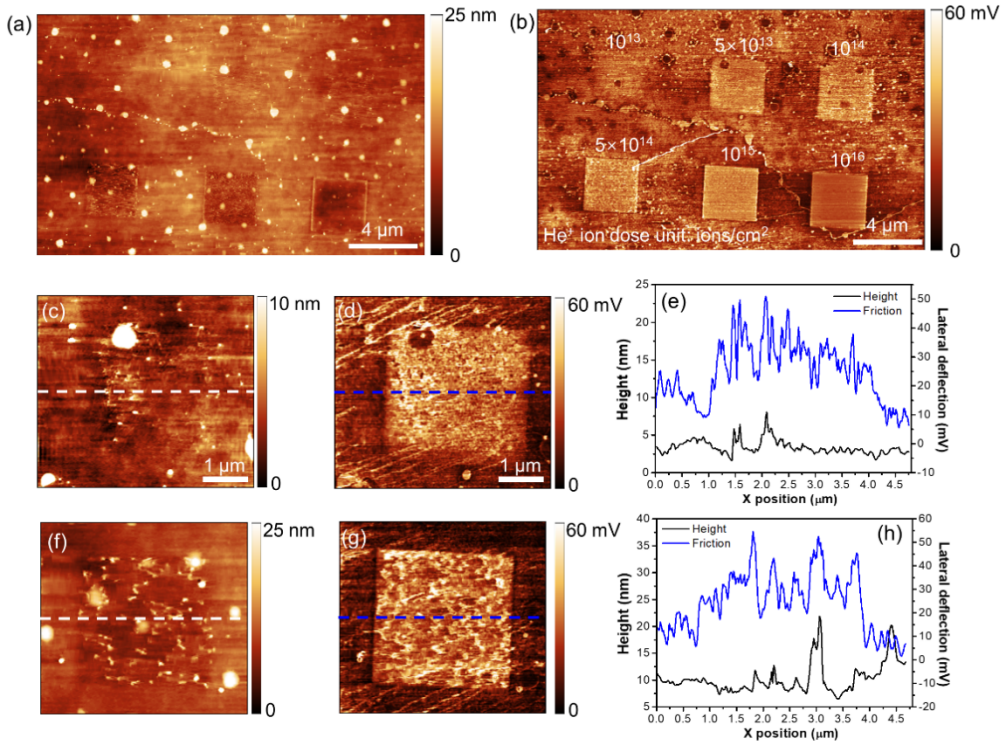

Figure S4. (a) Surface topography and (b) friction images of the second set of the helium ion irradiation experiments. (c), (d) High-resolution surface topography and friction images after the ion irradiation at a dose of 5×10^{13} ions/cm^2 and (e) the corresponding surface line profiles, and (f) surface topography (g) friction images after the ion irradiation at a dose of 5×10^{14} ions/cm^2 and (h) the corresponding surface line profiles.

Figure S4 shows the result for the second set of the helium ion irradiation experiments with the ion doses from 10^{13} to 10^{16} ions/cm^2. The resulting square patterns were measured using FFM. Figure S4(a) shows there was no significant surface topographic change for square patterns irradiated with ion doses from 10^{13} to 5×10^{14} ions/cm^2, whereas there were distinct changes in surface topography images with ion doses of 10^{15} and 10^{16} ions/cm^2. Figure S4(b) shows the lateral deflection image of the MoS_2 film corresponding to the surface topography image in Figure S4(a). There were significant frictional

signal changes for patterns irradiated with ion doses from 5×10^{13} to 10^{16} ions/cm^2, while there was only slight change with ion doses of 10^{13} ions/cm^2. With ion doses of 10^{16} ions/cm^2, frictional signal became similar with that of underlying SiO_2/Si substrate, which indicates MoS_2 can be milled out with this ion dose. Figures S4(c)~S4(h) show the high-resolution AFM images and cross-sectional profiles for the square patterns irradiated with ion doses of 5×10^{13} ions/cm^2 and 5×10^{14} ions/cm^2. Figure S4 (c), (f) shows there was no surface topographic change at low ion dose, while there were significant frictional signal changes in both low and high ion doses as shown in Figures S4(d) and S4(g).